Proceedings of the 9th U.S. National and 10th Canadian Conference on Earthquake Engineering
Compte Rendu de la 9ième Conférence Nationale Américaine et
10ième Conférence Canadienne de Génie Parasismique
July 25-29, 2010, Toronto, Ontario, Canada • Paper No 1060

MODELING THE DEGRADING SHEAR BEHAVIOR OF REINFORCED CONCRETE COLUMNS TO COLLAPSE

M. R. LeBorgne[1] and W. M. Ghannoum[2]

ABSTRACT

A self-calibrating shear failure model for non-seismically detailed reinforced concrete columns has been developed and implemented analytically. The proposed model is capable of detecting shear failure in columns and simulating inelastic shear deformations and strength loss to residual shear capacity. Shear failure is identified when the rotations across the plastic hinge of the column reach a critical value defined by an experimentally calibrated rotation based limit curve. Upon shear failure initiation, a zero-length shear spring connected in series with the column elements changes its constitutive properties to include pinching, strength degradation, and stiffness degradation. Shear spring constitutive properties are related to column material and geometric properties through least squares regressions. Preliminary comparisons show the model fits well with experimental data.

Introduction

Non-seismically detailed reinforced concrete (RC) columns such as those used in pre-1970's moment frame construction are highly prevalent in the United-States and around the world. The poor seismic performance of such columns is a major contributor to collapse of RC structures during large seismic events. Column collapse can be caused by axial overloading, excessive lateral deformations, or a combination of both. Assessing seismic collapse behavior of RC frames necessitates adequate modeling of lateral load behavior of columns up to large deformations. Specifically, degrading shear strength behavior of columns needs to be adequately modeled if lateral load sharing between structural elements is to be assessed with reasonable accuracy during seismic excitation. Furthermore, it has been observed that axial failure occurs when shear resistance degrades substantially (Yoshimura 2000). Therefore, estimating lateral damage progression results in a better assessment of global structural stiffness and when axial collapse is initiated.

An analytical model is proposed that is capable of simulating post shear failure behavior in non-seismically detailed RC columns that yield in flexure prior to initiating shear strength

[1] Graduate Research Assistant, Dept. of Civil Engineering, University of Texas, Austin, TX 78758
[2] Assistant Professor, Dept. of Civil Engineering, University of Texas, Austin, TX 78758

degradation. This rotation based shear strength degradation model is implemented analytically using zero-length shear spring elements placed in series at the ends of the column flexural elements. The model is capable of triggering shear failure and can account for the ensuing nonlinear degrading behavior through the shear spring. Model parameters that control post shear failure behavior are calibrated to known column properties, and in cycle boundary conditions (axial load and shear stress). These parameters include pinching, reloading stiffness degradation, and strength degradation. The rotation based shear strength degradation model has been calibrated by running least squares regressions on model parameters extracted from the quasi-static load-deformation history of 47 RC columns.

Methods

An analytical framework for RC columns has been developed for extracting degradation (damage) parameters. Extraction of damage parameters requires the separation of column shear deformations from flexural deformations. The majority of column tests compiled in the database presented experimental results in the form of a global lateral load versus deformation relation. The global response includes both shear and flexural deformations. However, the strength degradation model only controls column shear deformations and damage parameters must be calibrated to the shear deformation behavior. Thus, an analytical separation of deformations had to be performed where by flexural deformations are estimated analytically and subtracted from reported global deformations to obtain shear deformations.

Analytical Model Framework

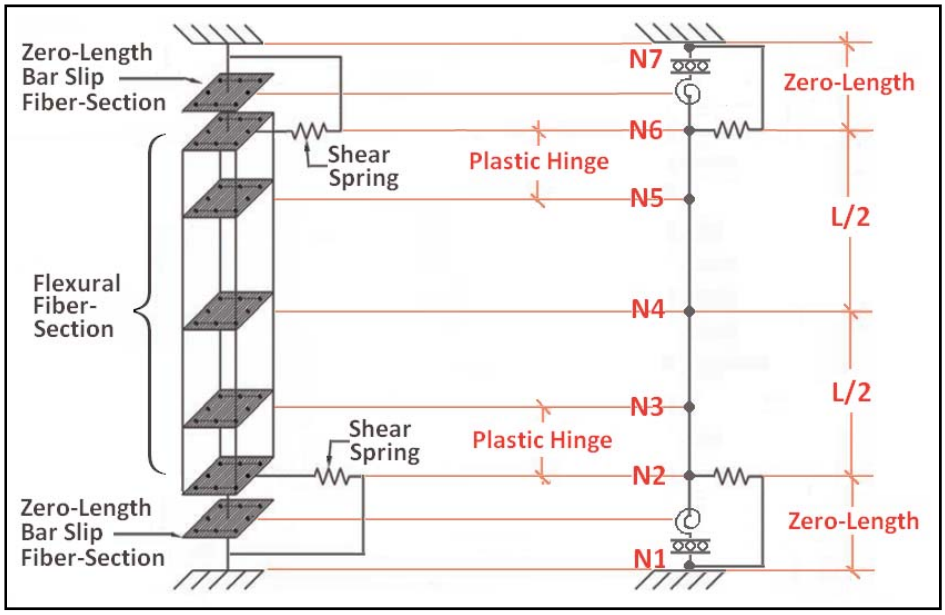

Figure 1. Analytical fiber section model to account for shear strength degradation.

To reduce error in shear deformation estimates, an accurate flexural model (Ghannoum 2007) was calibrated to fit column test data prior to shear failure initiation. All column analyses were performed using OpenSees (McKenna 1997), which is a modular open source earthquake simulation package. Column flexural response was modeled using fiber sections aggregated

within four flexibility-based nonlinear beam-column elements (see Fig. 1). As lateral load is applied to a column, the longitudinal bars will slip within the adjacent foundations due to strain penetration effects and cause the column to exhibit rigid body rotations (Sezen 2006). Bar slip induced rotations are accounted for by introducing a zero-length fiber-section element that is connected in series with column elements (Ghannoum 2007). Fiber sections in beam-column and bar slip elements can account for axial-flexure interaction but do not provide any shear resistance. Additional zero-length shear springs are connected in parallel to the zero-length bar slip fiber sections to account for the shear behavior. The shear springs incorporate the shear-deformation response of the proposed shear strength degradation model.

Shear failure initiation is triggered by the model when column end-rotations measured over the plastic hinge length (equal to the column section height) exceed the threshold value defined by a rotation based shear limit curve (Eq. 1). The rotation based limit curve compares the total rotation across the plastic hinge region including bar slip rotations to the total rotation limit (θ_{Total}). Eq. 1 was developed under a separate study (Ghannoum 2007). A list of terms is provided in the last section.

$$\theta_{Total} = 0.044 - 0.017\left(\frac{s}{d}\right) - 0.021\left(\frac{P}{A_g f_c^{'}}\right) - 0.002\left(\frac{v}{\sqrt{f_c^{'}}}\right) \geq 0.009 \tag{1}$$

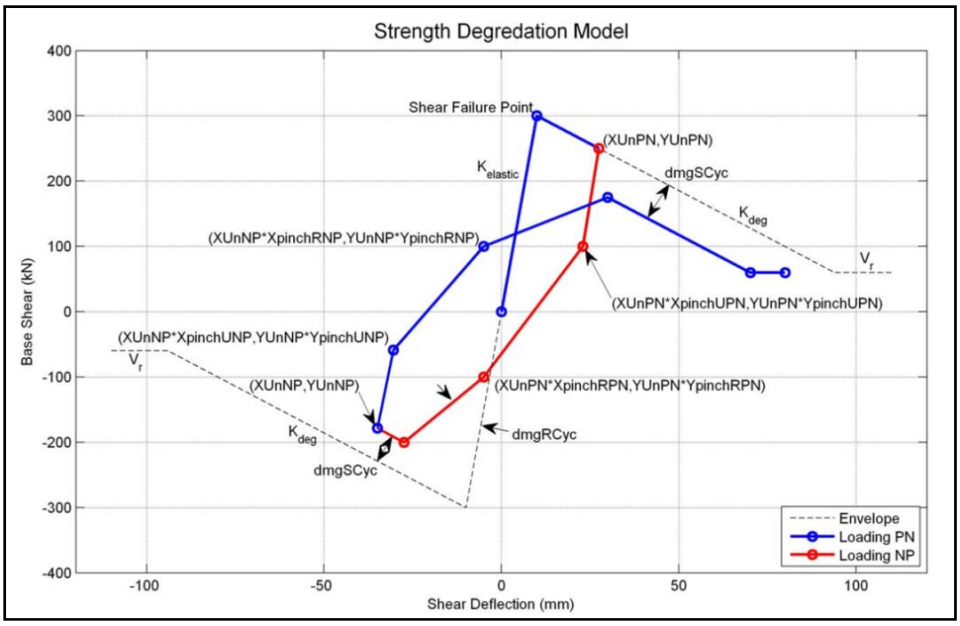

Figure 2. Effect of degradation parameters on the strength degradation model. The last two letters of the pinching coordinate indicate direction, PN for loading from the I quadrant to the III quadrant and NP if loading occurs in the opposite direction.

Once shear failure is detected by the rotation based limit curve, the constitutive properties of the shear spring are altered from elastic to nonlinear. The degrading shear behavior is calibrated to the experimental test data using six pinching variables, cyclic reloading stiffness damage, cyclic strength degradation damage, and a degrading slope. Model parameters

that are used in the calibration process are illustrated in Fig. 2. The proposed shear strength degradation model and the rotation based limit curve have both been implemented in the OpenSees framework as modular components.

The strength degradation model has several rules to determine its behavior. Prior to shear failure detection, the strength degradation model maintains an elastic slope ($K_{elastic}$). Once shear failure is detected, the model calculates envelope limits which represent the maximum load and deformation combinations the model can achieve. The shear strength envelope is defined by the point where shear failure is detected and the degrading slope (K_{deg}). At twenty percent of the load at shear failure, the envelope becomes flat at the column's estimated residual strength (V_r). Upon load reversal, the points which form the tri-linear pinching segments are defined. Pinching-point coordinates are defined as a fraction of loads and deformations at which load reversal occurs (Fig. 2). The unloading segment is assumed to be elastic and was found in this study to closely follow the initial elastic slope ($K_{elastic}$). Once the reloading point is reached, reloading stiffness damage is automatically enforced by not allowing the shear at unloading to be exceeded at reloading. A cyclic degradation factor (*dmgRCyc*) is used to further reduce the maximum achievable shear force beyond what is automatically calculated during reloading. At each reloading cycle, strength degradation (*dmgSCyc*) is applied to successively reduce the y-intercept of the envelope at each half cycle. This simple strength degradation scheme reproduced test results accurately and avoided the more complex energy or deformation based damage schemes that are difficult to calibrate given the available dataset. The proposed strength degradation model monitors the shear and deformation envelope at the global level for exceedance by tracking the flexural deformations between the column fiber sections. Monitoring global deformations gives the strength degradation model the ability to increase shear deformations while the flexural fiber section is unloading during cyclic strength degradation.

Parameter Extraction

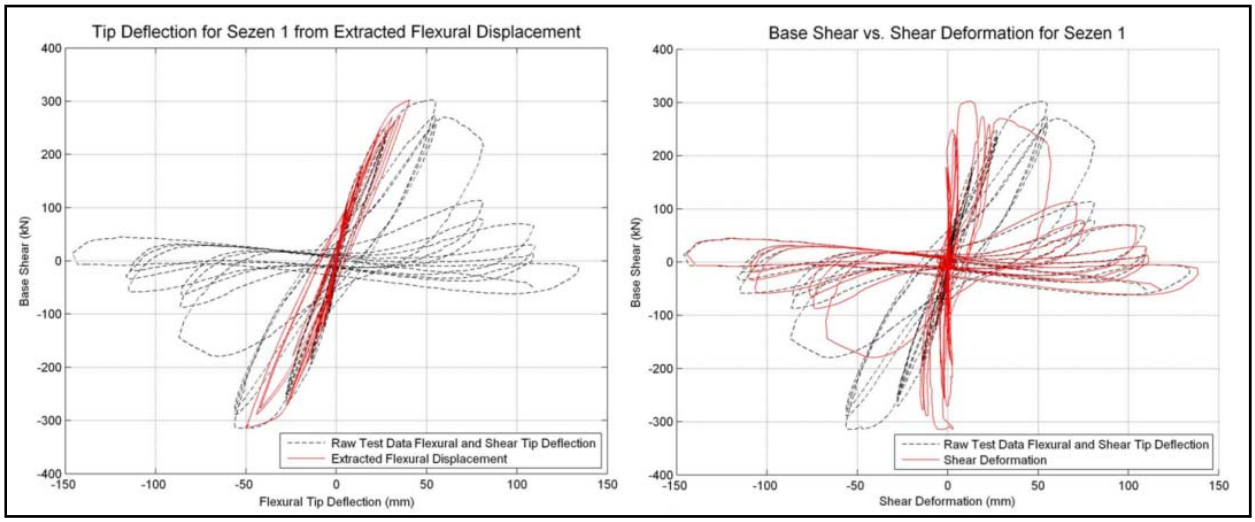

Figure 3. Flexural displacement and shear displacement for specimen 1 tested by Sezen.

The shear strength degradation model only controls shear deformations. Therefore, any damage parameters must be extracted from the column shear deformations. Approximate shear

deformations can be compiled by creating an accurate model of the flexural behavior using OpenSees and subtracting the flexural response from the experimental deformations. The fiber section element used in OpenSees can accurately represent the flexural behavior of the column and if the experimental lateral load history is applied to a column model in force control, it will produce the approximate flexural component of the column's experimental behavior. By subtracting the derived flexural deformations from the total measured deformations, an approximate shear deformation response indicative of a column's actual shear deformations is created. The shear curve computed for specimen 1 tested by Sezen is presented in Fig. 3 (Sezen 2006).

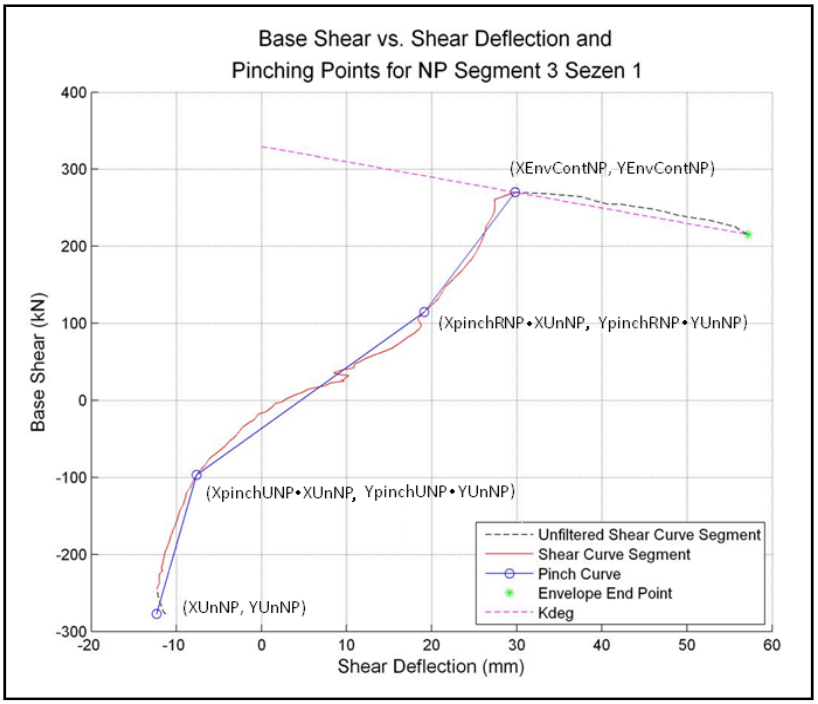

Figure 4. Base shear vs. shear deflection and pinching points for NP segment 3 for specimen 1 tested by Sezen.

Six pinching factors are extracted from the shear deformation history by breaking the shear curve into segments between unloading points. Segments are filtered to find the loading direction, unloading point, and envelope contact point. A tri-linear branch is fitted to the unloading and envelope contact points as shown in Fig. 4. The two intermediate pinching points along the tri-linear branch are found by iterating all possible point combinations along the shear curve. Then the area under the experimental shear curve and tri-linear pinching curve are compared. A point combination that produces the minimum difference in areas is chosen as a match for the current segment. Calculated pinching points are segregated depending on loading direction. Pinching ratios are calculated as a fraction of the unloading point. They are then averaged to obtain the mean pinching factor for a column shear deformation history. There are three mean pinching ratios for each segment which include *YpinchU*, *XpinchR*, and *YpinchR*. The fourth pinching ratio, *XpinchU*, is calculated by the shear strength degradation model using the elastic unloading slope ($K_{elastic}$) and *YpinchU*.

The shape of the envelope which limits the strength and deformation of the column cannot be fully defined due to the limited number of tests conducted monotonically to collapse. Thus the shape of the envelope was approximated as a linear segment with a slope equal to K_{deg}. Due to the cyclic nature of most tests, the envelope is only contacted for short deformation periods giving only a brief glimpse of its true shape. The sporadic envelope contact requires the degrading slope to be extracted by breaking the shear curve into segments and capturing the envelope between the envelope contact point defined by (*EnvCont*) and the unloading point. The envelope contact point is identified as the location where softening begins during reloading (see Fig. 4). The mean value of the degrading slope for all the segments is recorded as K_{deg}.

The strength damage parameter (*dmgSCyc*) is extracted from the shear curve segments. An algorithm was developed to calculate the y-intercept of the degrading slope and determine the amount the envelope has shifted between segments. The value of the envelope shift is the amount of strength degradation incurred per half cycle. The strength degradation per half cycle is normalized as one minus the ratio of the y-intercept of the current half cycle to the y-intercept of the previous half cycle. An average is taken of the normalized strength damage parameters for all segments. The mean value recorded for each column is the approximate strength damage incurred at each half cycle. Reloading stiffness damage (*dmgRCyc*) reduces the stiffness of the reloading slope during the pinching algorithm. If two consecutive segments of the shear curve contact the envelope, the reloading stiffness damage can be determined by taking one minus the ratio of the reloading shear at envelope contact (*YEnvCont*) to the unloading shear (*YUn*).

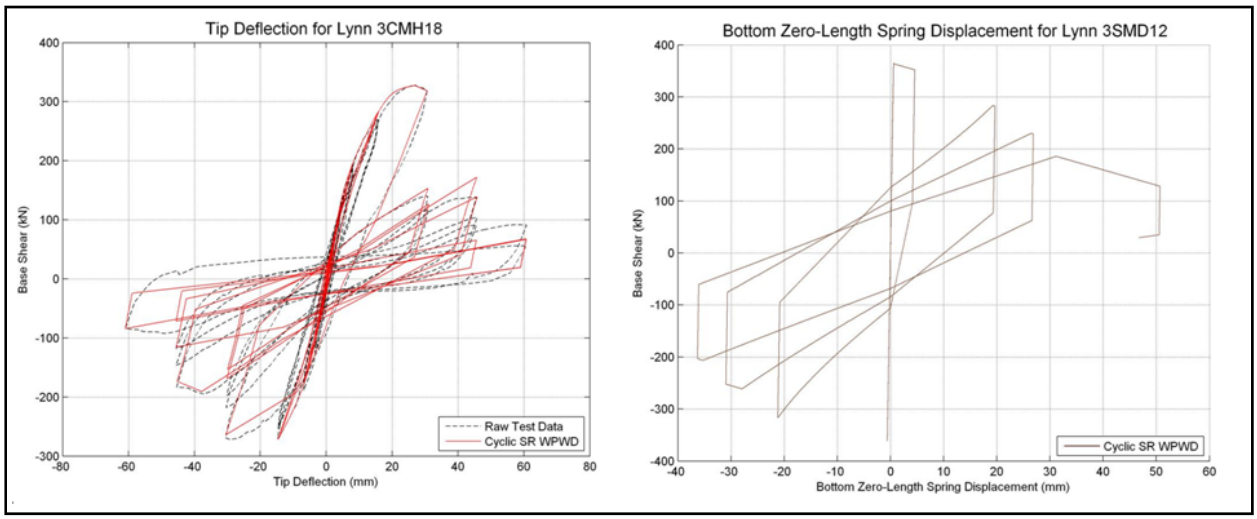

Figure 5. Fitted strength degradation model for a column 3CMH18 tested by Lynn.

The algorithms presented to extract the pinching and damage parameters from the experimental data were an asset in determining the final pinching and damage parameters. However, iterative manual manipulation of the pinching and damage parameters was undertaken to achieve the best possible fit. As a result of the manual manipulation it was found that multiple sets of pinching parameters could produce acceptable results. A sample of the fitted results using the strength degradation model is shown in Fig. 5 for column 3CMH18 tested by Lynn (Lynn 2001). The tip deflection and the shear deformation produced by the shear strength degradation model are shown in Fig. 5.

Results

Preliminary Trends

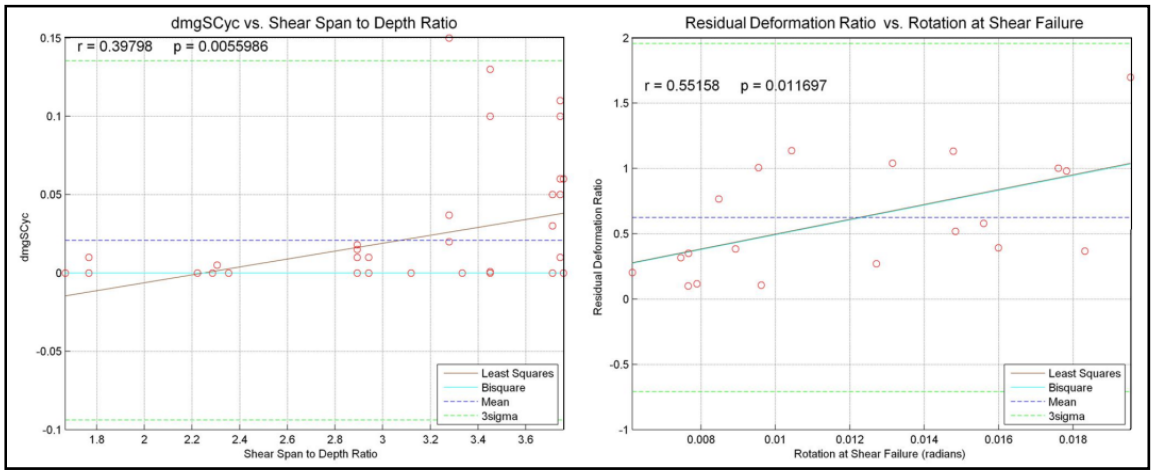

Figure 6. Correlations found between predictor and response variables.

Model degradation parameters (response variables) were plotted against pertinent normalized predictor variables. Predictor variables with a correlation p-value less than 0.15 had adequate correlation with the response variables and were kept for further statistical investigation (Fig. 6). To reduce the variance between predictor and response variables a stepwise regression was conducted. The stepwise regression was performed multiple times for each response variable starting with a different predictor variable for each regression. The order of the predictors in the stepwise regression that showed the lowest root mean squared error (RMSE) were used to determine the sequence with which each predictor was added to the partial least square regression. Plots of the percent variance explained for each response variable were produced. Any normalized predictor that did not substantially increase the explained variance was dropped.

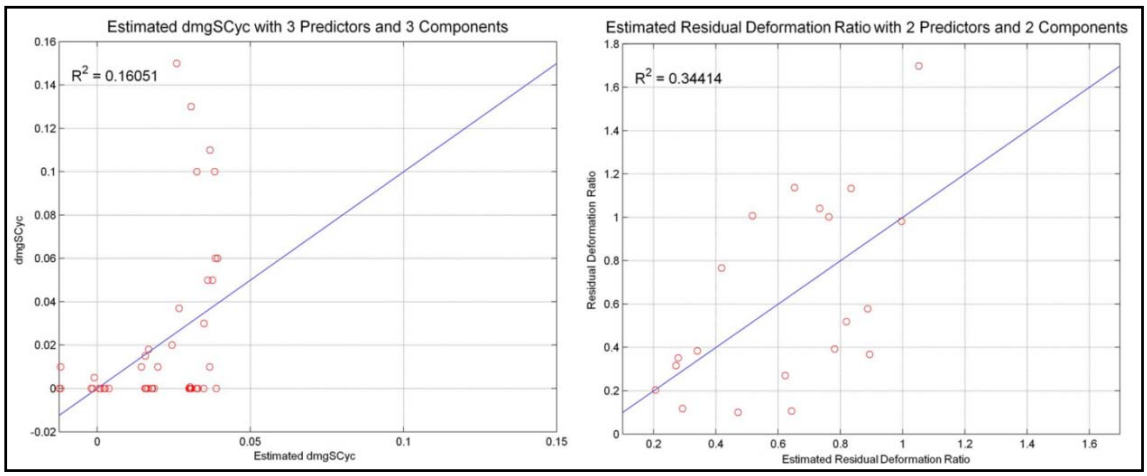

Figure 7. Estimated strength damage (*dmgSCyc*) and deformation ratio (Δ_r/h) plotted against the experimental data.

The statistical analysis for reloading stiffness damage (*dmgRCyc*) showed significant variation and no clear trends. Plots of the data showed the majority of the values at zero, hence the reloading strength damage was set as a constant equal to zero. The cyclic strength damage parameter (*dmgSCyc*) exhibited good correlation with certain predictor variables as shown in Fig. 7. A preliminary equation derived from a linear regression for the parameter is reproduced in Eq. 2. Further investigation needs to be performed on this parameter to verify that a linear regression is the most appropriate relational form between the predictor and response variables.

$$dmgSCyc = -0.0776 \; + \; 0.02954 \cdot \frac{s}{d} + 0.06023 \cdot \frac{v}{f_c'} + 0.5247 \cdot \rho_t \geq 0.0 \tag{2}$$

To normalize the degrading slope (K_{deg}) it is necessary to estimate shear deformations from point of shear failure initiation to a point along the envelope where shear strength is zero. This distance can then be normalized by dividing it by column section-height as shown in Eq. 3 to obtain the residual deformation ratio (Δ_r/h). Experimental test setups affect the degrading slope that is captured by the parameter extraction algorithms. The regression of the residual deformation ratio shown in Eq. 4 uses only columns tested in double curvature. A plot of the extracted residual deformation ratio and the estimated residual deformation ratio is shown in Fig.7.

$$\frac{\Delta_r}{h} = \frac{V_f}{K_{\deg} \cdot h} \tag{3}$$

$$\frac{\Delta_r}{h} = 0.2054 \; + \; 48.492 \cdot \theta_f - 0.2563 \cdot \frac{s}{d} \geq 0.036 \tag{4}$$

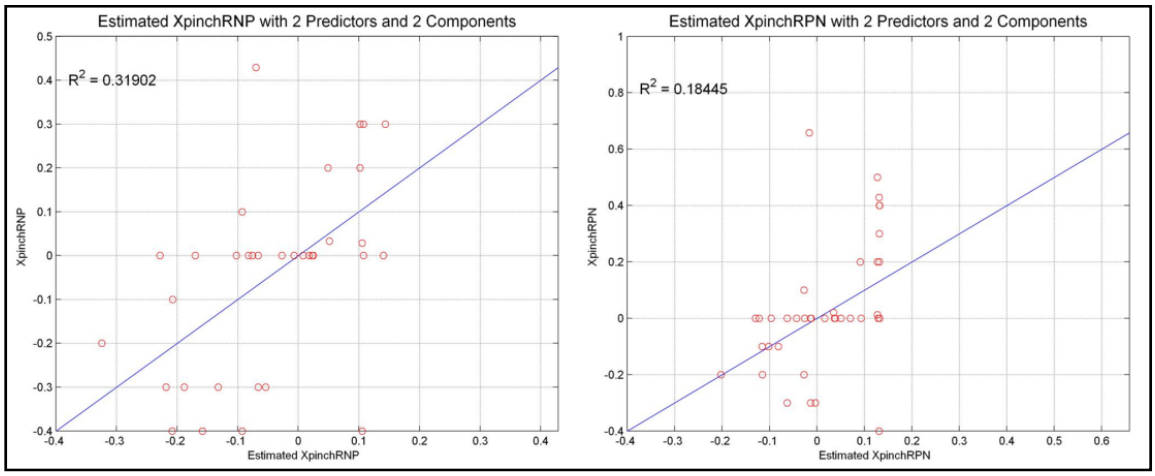

Figure 8. Estimated deformation pinching factors for reloading (*XpinchRNP and XpinchRPN*) plotted against the experimental data.

Pinching factors (*XpinchRNP and XpinchRPN*) exhibited some correlation with predictor variables as shown by the plots in Fig. 8. The resulting equations from the partial least squares regression are shown in Eqs. 5 and 6. Strong trends were not observed between reloading shear pinching factors (*YpinchRNP and YpinchRPN*) and normalized predictor variables. However, reloading shear pinching factors did exhibit correlation with their respective shear displacement

pinching factors. The resulting robust regressions of the shear pinching factors are shown in Eqs. 7 and 8. The unloading pinching shear factors (*YpinchUNP and YpinchUPN*) showed no trends with respect to predictor variables. Thus unloading shear factors were set as constants equal to their mean value of 0.3.

$$XpinchRNP = 0.1707 + 0.3508 \cdot \frac{s}{d} - 0.6259 \cdot \frac{A_{cc}}{A_g} \tag{5}$$

$$XpinchRPN = 0.2068 - 0.5107 \cdot \frac{A_{cc}}{A_g} + 0.2403 \cdot \frac{s}{d} \tag{6}$$

$$YpinchRNP = 0.3471 + 0.5831 \cdot XpinchRNP \tag{7}$$

$$YpinchRPN = 0.3114 + .4465 \cdot XpinchRPN \tag{8}$$

Results of the preliminary implementation of the calibrated rotation-based shear strength degradation model are shown in Fig. 9 for specimens 2D16-R-S (Ohue 1985) and H-2-1-3 (Esaki 1996). Fig. 9 shows the level of accuracy that the proposed self calibrating rotation base shear strength degredation model can achieve.

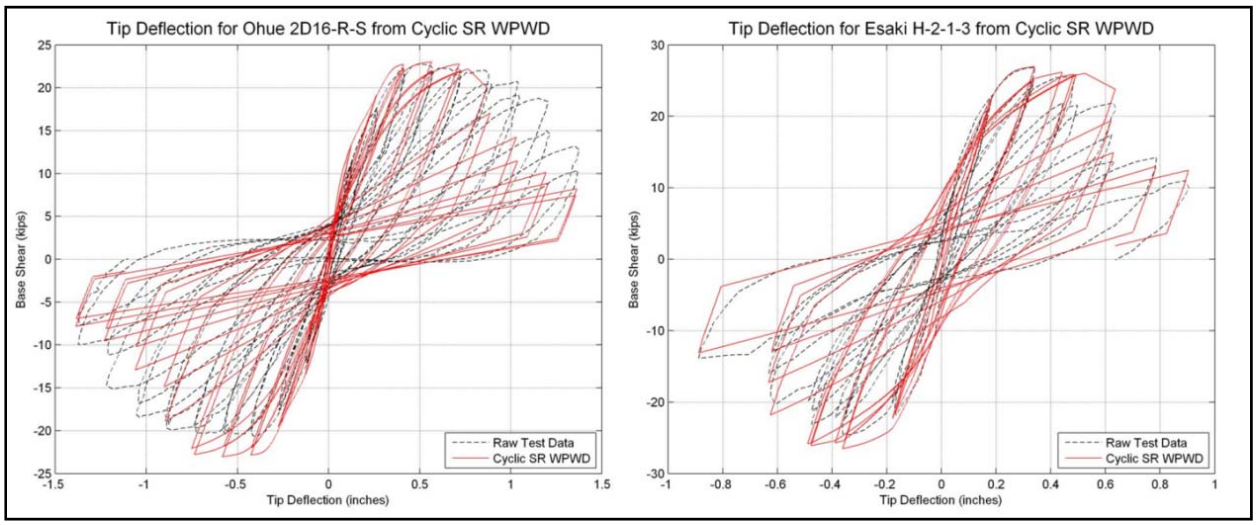

Figure 9. Preliminary results of the rotation based shear strength degradation model applied to specimens 2D16-R-S tested by Ohue et al. and H-2-1-3 tested by Esaki.

Conclusions

The proposed rotation-based shear failure model has been calibrated to detect shear failure in non-seismically detailed RC columns and estimate nonlinear post shear-failure behavior. Preliminary results show that presented relations can adequately predict model parameters so long as the column properties are within the material and geometric parameters of the database. The benefit of the fully functional rotation based strength degradation model will result in less user judgment in assigning fitting parameters and less variability in the final model. More work is still needed to refine relations between model parameters and predictor variables.

List of Terms

Term	Description	Database Limits			
		Min	Mean	Max	Unit
s/d	Transverse reinforcement spacing to column depth ratio	0.1	0.6	1.1	-
b	Width of column cross section	151	265	550	mm
d	Section depth to the tension reinforcement	169	258	476	mm
a/d	Shear span to depth ratio	1.7	3.0	3.8	-
$f_c^{'}$	Compressive strength of concrete	18	27	47	MPa
ρ_t	Transverse reinforcement ratio	0.0007	0.0037	0.014	-
A_{cc}/A_g	Confined concrete to gross section area ratio	0.38	0.64	0.86	-
P	Axial load on column (positive for compression)	0	417	1800	kN
K_{deg}	Degrading slope measured from shear curve	-12.0	-2.5	-0.4	kN/mm
v	Stress at shear failure = (shear at failure) $/(b \cdot d)$	1.3	2.4	4.0	MPa
θ_f	Analytically measured rotation across the plastic hinge including bar-slip at shear failure	0.006	0.019	0.067	Rad.

References

Elwood, K. J., and Moehle, J. P. (2005). "Axial Capacity Model for Shear-Damaged Columns." *ACI Structural Journal*, 102(4), 578-587.

Esaki, F., 1996. Reinforcing Effect of Steel Plate Hoops on Ductility of R/C Square Column, *Eleventh World Conference on Earthquake Engineering,* Paper No. 199.

Ghannoum, W. M., 2007. Experimental and Analytical Dynamic Collapse Study of a Reinforced Concrete Frame with Light Transverse Reinforcement, *PhD Thesis*, University of California, Berkeley.

Lynn, A. K., 2001. Seismic Evaluation of Existing Reinforced Concrete Building Columns, *PhD Thesis*, University of California, Berkeley.

McKenna, F. T., 1997. Object-Oriented Finite Element Programming: Frameworks for Analysis, Algorithms and Parallel Computing, *PhD Thesis*, University of California, Berkeley.

Ohue, M., H. Morimoto, S. Fujii, and S. Morita, 1985. The Behavior of R.C. Short Columns Failing in Splitting Bond-Shear Under Dynamic Lateral Loading, *Transactions of the Japan Concrete Institute* 7, 293-300.

Sezen, H., and Moehle, J. P. 2006. Seismic Tests of Concrete Columns with Light Transverse Reinforcement. *ACI Structural Journal*, 103(6), 842-849.

Yoshimura, M., and Yamanaka, N. 2000). "Ultimate Limit State of RC Columns." *Proceedings of the Second U.S.-Japan Workshop on Performance-Based Earthquake Engineering Methodology for Reinforced Concrete Building Structures*, Sapporo, Hokkaido, Japan, 313-326.